Science and Technology of Advanced Materials

ISSN: (Print) (Online) Journal homepage: www.tandfonline.com/journals/tsta20

Enhanced laser-induced single-cycle terahertz generation in a spintronic emitter with a gradient interface

Leonid Andreevich Shelukhin, Anna Vasilevna Kuzikova, Andrey Vladimirovich Telegin, Vladimir Dmitrievich Bessonov, Alexey Viacheslavovich Ognev, Alexander Sergeyevich Samardak, Junho Park, Young Keun Kim & Alexandra Mikhailovna Kalashnikova

To cite this article: Leonid Andreevich Shelukhin, Anna Vasilevna Kuzikova, Andrey Vladimirovich Telegin, Vladimir Dmitrievich Bessonov, Alexey Viacheslavovich Ognev, Alexander Sergeyevich Samardak, Junho Park, Young Keun Kim & Alexandra Mikhailovna Kalashnikova (31 Jan 2025): Enhanced laser-induced single-cycle terahertz generation in a spintronic emitter with a gradient interface, Science and Technology of Advanced Materials, DOI: 10.1080/14686996.2024.2448417

To link to this article: https://doi.org/10.1080/14686996.2024.2448417

Accepted author version posted online: 31 Jan 2025.

Publisher: Taylor & Francis & The Author(s). Published by National Institute for Materials Science in partnership with Taylor & Francis Group.
Journal: *Science and Technology of Advanced Materials*
DOI: 10.1080/14686996.2024.2448417

Enhanced laser-induced single-cycle terahertz generation in a spintronic emitter with a gradient interface

Leonid Andreevich Shelukhin[a*], Anna Vasilevna Kuzikova[a], Andrey Vladimirovich Telegin[b], Vladimir Dmitrievich Bessonov[b], Alexey Viacheslavovich Ognev[c, d], Alexander Sergeyevich Samardak[c, d], Junho Park[e], Young Keun Kim[e*], Alexandra Mikhailovna Kalashnikova[a]

[a]Ioffe Institute, 194021 St. Petersburg, Russia; [b]M. N. Mikheev Institute of Metal Physics, Ural Branch of Russian Academy of Science, 620108, Yekaterinburg, Russia; [c]Far Eastern Federal University, 690922, Vladivostok, Russia; [d] Sakhalin State University, Yuzhno–Sakhalinsk, 693000, Russia; [e]Department of Materials Science and Engineering, Korea University, Seoul 02841, Republic of Korea

ABSTRACT

The development of spintronic emitters of broadband terahertz (THz) pulses relies on designing heterostructures in which the processes of laser-driven spin current generation and subsequent spin-to-charge current conversion are the most efficient. The interface between the ferromagnetic and nonmagnetic layers in an emitter is a critical element. In this study, we experimentally examined single-cycle THz pulse generation from a laser-pulse-excited Pt/Co emitter with a 1.2-nm-thick composition-gradient interface between the Pt and Co and compared it with the emission from a conventional Pt/Co structure with an abrupt interface. We found that the gradient interface improved the efficiency of the optics-to-THz conversion by a factor of two in a wide range of optical fluences up to 3 $mJ \cdot cm^{-2}$. This enhancement was caused by a pronounced increase in the transmittance of the laser-driven spin-polarized current through the gradient interface compared with the abrupt interface. Moreover, it was evident that such transmission deteriorated with the laser fluence owing to the spin accumulation effect.

ARTICLE HISTORY

Compiled November 28, 2024

KEYWORDS

spintronic emitter, single-cycle terahertz pulse, inverse spin Hall effect, Pt/Co interface

CONTACT Leonid Andreevich Shelukhin shelukhin@mail.ioffe.ru Ioffe Institute, 194021 St. Petersburg, Russia; Young Keun Kim ykim97@korea.ac.kr Department of Materials Science and Engineering, Korea University, 145 Anam-ro, Seongbuk-gu, Seoul 02841, Republic of Korea

Introduction

The demand for broadband THz emitters for various applications [1] has led to considerable progress in the field, with emitters based on various materials and operating under different principles [2–11]. Multilayer spintronic structures that convert laser-driven spin dynamics into picosecond charge currents [12] make promising single-cycle THz sources [5,13–19]. The foremost spintronic emitters based on nonmagnetic metal/ferromagnetic metal (NM/FM) heterostructures rely on spin/charge conversion by the inverse spin Hall effect (ISHE) occurring in the bulk of the NM layer, which possesses strong spin-orbit coupling [20,21]. Therefore, optimizing the thicknesses and materials of the NM and FM layers is vital to obtaining a major increase in THz emission in spintronic emitters [5]. Interfaces in such structures have been found to be an alternative source of THz emission, enabled by symmetry breaking [22,23], the Rashba–Edelstein effect [24], and skew scattering by impurities [25].

Nevertheless, interfaces in NM/FM heterostructures can have a strong impact — even on the "bulk" spin-to-charge conversion — because of their influence on the spin and spin-mixing conductance [26–29] and spin memory loss [30–33]. The manipulation of THz emission by adding nonmagnetic interfacial layers [26] or intermixing [25,34,35] at the NM/FM interface of a spintronic emitter has also been reported. It has been established that the THz emission in these modified structures correlates with changes in interface-related spin phenomena like spin pumping [26]. Consequently, examining the THz emission properties of structures with designs that enable the enhancement of particular interface-related spintronic phenomena could be a promising research direction.

In this study, we explored a n approach to boost the THz generation of a spintronic emitter through an advanced Pt/Co interface design. The interfacial layer between the Co and Pt — which comprises a Pt/Co content gradient — makes the interface less abrupt than that of a conventional Co/Pt emitter. Interestingly, such structures with a gradient interface demonstrate an approximately two-fold enhancement of the interfacial spin phenomenon via the Dzyaloshinskii–Moriya interaction (DMI) [36]. We demonstrated that such an interface led to a nearly two-fold increase in the optical-to-terahertz fluence conversion efficiency compared to a Pt/Co emitter with the same layer thickness and sharp interface. By excluding the effect of the thickness change and quantifying the spin current generated in the Co layer by ultrafast demagnetization measurements, we concluded that the main role in enhancing THz generation was the increased spin transmittance of the gradient interface to a spin current.

Experimental Methods

Sample preparation and characterization

Two primary samples of spintronic THz emitters were examined; in other words, the conventional Pt(3)/Co(1.2) structure with an abrupt interface (numbers in brackets indicate the thicknesses in nm), and the Pt(3)/g-PtCo(1.2)/Co(1.2) structure with a 1.2-nm-thick composition-gradient interface (g-PtCo) between the NM and FM layers having a nominal composition $Co_{25}Pt_{75}$(0.4)/$Co_{50}Pt_{50}$(0.4)/$Co_{75}Pt_{25}$(0.4). Three different alloys ($Co_{25}Pt_{75}$, $Co_{50}Pt_{50}$ and $Co_{75}Pt_{25}$) were utilized for the deposition of the g-PtCo. The Pt and Co layer thicknesses (**Table 1**) were chosen to be close to the respective optima for THz emission

[15,37]. Single films of the Co(4.6) and $Co_{75}Pt_{25}$(4.6) alloys and spintronic emitters $Co_{75}Pt_{25}$(4.2)/Co(0.8), $Co_{50}Pt_{50}$(4.2)/Co(0.8), and Pt(2)/$Co_{75}Pt_{25}$(4.2) were used as references. All samples were fabricated on Si substrates with about 300-nm-thick thermal oxides using UHV DC magnetron sputtering at a base pressure of 5×10^{-9} Torr at room temperature and then post-annealed at 300 °C for 1 h in a vacuum of 1×10^{-9} Torr [36]. The bottom 2-nm and top 2-nm Ta layers were deposited as buffer and capping layers, respectively. The Pt/g-PtCo/Co sample structure is schematically shown in **Figure 1(a)**.

Transmission electron microscopy (TEM) and X-ray diffraction studies showed that the samples possessed an *fcc* (111) structure [36]. TEM study also revealed that the interfacial layer g-PtCo was characterized by a gradual change in the Co-Pt content ratio rather than a step one [36].

Information on the magnetization and magnetic anisotropy of the samples is summarized in **Table 1**, as obtained from vibrating-sample magnetometry measurements. As expected, changing the composition of the FM layers, adding a Pt layer, and modifying the interface resulted in variations in the strength and sign of the magnetic anisotropy [38,39]. Notably, the addition of a gradient interface to the Pt/Co led to a change in the magnetic anisotropy from out-of-plane to in-plane, which is optimal for spintronic emitters. The magnetization hysteresis loops obtained in the in-plane magnetic field for Pt/Co and Pt/g-PtCo/Co samples are shown in **Figure 2(a)**. **Table 1** lists the DMI parameters of the samples reported in Ref. [36].

THz emission

In the THz emission experiment, laser pump pulses with a central wavelength of 800 nm and a repetition rate of 1 kHz were generated using a Ti:sapphire regenerative amplifier. They were collimated into a 1-mm-diameter spot on the sample surface, providing a fluence ranging from 0.01–3 $mJ \cdot cm^{-2}$. Excitation was performed on the side of the structure, and the THz emission was studied after passing through the substrate [**Figure 1(a)**]. The resulting THz pulse waveform was detected by electro-optical sampling [40] using a 1-mm-thick ZnTe crystal with (111) orientation. ZnTe was selected because its high electro-optical coefficient enabled the detection of weak THz fields. The electro-optical coefficient of the ZnTe crystal was verified using control measurements with a 200-μm (110)-oriented GaP crystal. To set the magnetization state of the sample, an external magnetic field $\mu_0 H$ = 50–750 mT was applied in the sample plane, with $\mu_0 H$ = 750 mT sufficient for the in-plane saturation of all samples, including those with perpendicular magnetic anisotropy [**Figure 2(a)**]. All measurements were performed in a dry nitrogen atmosphere with humidity below 10%.

Ultrafast demagnetization

Ultrafast laser-induced demagnetization was measured using the time-resolved longitudinal magneto-optical Kerr effect scheme [41]. The Yb^{3+}:$KGd(WO_4)_2$ regenerative amplifier was the source of pump and probe pulses with a duration of 170 fs emitted at a repetition rate of 5 kHz. The central wavelength of the pump was converted to 800 nm using an optical parametric amplifier to reproduce laser excitation in the THz emission experiment. The pump pulses were focused normally onto the sample surface in an area of with a diameter of

40 μm, and their fluence was varied between 0 and 3 mJ $\cdot$ cm^{-2} (to match the conditions of the THz experiments) and up to 12.5 mJ $\cdot$ cm^{-2}. The central wavelength of the probe was converted to 515 nm using a beta-barium borate (BBO) crystal, enabling filtering of the pump pulses in front of the detector. The probe pulses had a fluence 50 times less than those of the pump pulses and were focused onto a spot of diameter 30 μm at an incidence angle of 45°. An external magnetic field of $\mu_0 H$ = 750 mT was applied in the sample plane. Rotation of the probe polarization plane was measured as a function of the time delay (Δt) between the pump and probe pulses using a balanced photodetector in combination with a Wollaston prism. The rotation of the probe polarization was proportional to the pump-induced change in magnetization saturation along the external magnetic field. The data were normalized using static magneto-optical Kerr rotation at saturation to determine the relative demagnetization magnitudes. Absolute values of the magnetization change ΔM were obtained from the normalized pump-probe data using static M_S and assuming that the signal was dominated by Co demagnetization.

Results

Typical THz waveforms from the Pt/Co and Pt/g-PtCo/Co measured in the in-plane external field $\mu_0 H$ = 750 mT under the optical fluence F = 3 mJ $\cdot$ cm^{-2} are shown in **Figure 1(c)**. The generated THz waveforms were independent of the laser pulse polarization, the THz emission being linearly polarized orthogonally to the applied field direction. The spectra obtained using fast Fourier transforms of the waveforms were similar for both samples [**Figure 1(b)**]. The spectra were limited by the sensitivity of the ZnTe crystal, and the small dip at 1.6 THz could be attributed to the features of this crystal [42]. To quantify the THz signals, we designated the largest deviation of the electric field from zero as the peak THz field, $E_{\mathrm{THz}}^{\mathrm{peak}}$ [**Figure 1(c)**]. In both the Pt/g-PtCo/Co and Pt/Co structures, $E_{\mathrm{THz}}^{\mathrm{peak}}$ reached a maximum value and saturated as the magnetization was saturated in the sample plane, as is evident from the field dependences of M and $E_{\mathrm{THz}}^{\mathrm{peak}}$, as shown in **Figure 2(a**). Notably, the temporal profiles of the THz pulses remained unchanged under different experimental conditions. Thus, the discussion holds true for the peak-to-peak values of the THz electric field that are often used in the literature.

These features, along with reversal of the THz pulse polarity with the magnetic field sign change [see the inset in **Figure 1(c)**], are characteristic of the emission originating from the ISHE in the Pt layer, as shown schematically in **Figure 1(a)**, or ultrafast demagnetization of the Co itself [4,43–48]. To verify that the origin of the THz signal in these two samples was spin-charge conversion by the ISHE, we compared the signals to those from the reference Co and $Co_{75}Pt_{25}$ samples, where ultrafast demagnetization was the dominant THz source [43]. The signals in the latter samples were 10–15 times lower in agreement with previous findings [28] and were of the opposite polarity compared to the signals in the Pt/g-PtCo/Co and Pt/Co [the orange and green curves shown in **Figure 1(d)**]. The fact that spin-to-charge conversion was a leading effect, whereas ultrafast demagnetization itself just corrected the THz field amplitude in the structures with a Pt layer, was further evident from the enhancement of $E_{\mathrm{THz}}^{\mathrm{peak}}$ and the reversal of the polarity in Pt/$Co_{75}Pt_{25}$, i.e., when the Pt layer was added to a thick $Co_{75}Pt_{25}$ layer [the violet curve in **Figure 1(d)**]. An additional check of the ISHE mechanism involved reversing the THz pulse polarity upon reversal of the

sample. This experiment was not possible with the studied samples because the Si substrate strongly absorbed the pump pulses.

We also addressed the possible role of Ta capping and buffer layers in all the structures. They could give rise to THz emission via the ISHE effect because the spin Hall angle of Ta was opposite in sign and approximately 10 times smaller than that of Pt. However, in single FM layer structures, the contributions from the two Ta layers cancelled each other because of the opposing directions of the injected spin currents [28]. In the NM/FM structures, the capping Ta layer adjacent to the Co layer provided a small positive correction to $E_{\mathrm{THz}}^{\mathrm{peak}}$. This correction was partly compensated for by the contribution from the buffer Ta layer with a weaker spin current.

Discussion

The above observations bring us to consider the processes responsible for the effective enhancement of different stages of THz generation via the ISHE in the Pt/g-PtCo/Co compared to Pt/Co. At $\mu_0 H$ = 750 mT both samples were saturated in the plane [**Figure 2(a)**], and a quantitative comparison of $E_{\mathrm{THz}}^{\mathrm{peak}}$ obtained under such conditions could be made. As is evident from **Figure 1(c)**, $E_{\mathrm{THz}}^{\mathrm{peak}}$ obtained from the Pt/g-PtCo/Co sample was ≈1.7 times higher than that emitted by Pt/Co at $F = 3\ \mathrm{mJ \cdot cm^{-2}}$.

Three processes potentially lead to the observed enhancement. First, the magnetically ordered Co-Pt alloys at the interface in Pt/g-PtCo/Co were an additional spin current source; second, the Co-Pt interfacial layers contributed to the emission of the THz pulse because of spin-to-charge conversion via the ISHE; finally, the interface in Pt/g-PtCo/Co possess a higher transmittance for the spin current moving from the Co-containing layers to the Pt film.

The fact that the g-PtCo layer added between the Pt and Co could serve as a source of spin current was evident from a comparison of the ultrafast demagnetization data closely related to the spin current [45] for the pairs of Co and $Co_{75}Pt_{25}$ samples. Ultrafast demagnetization measurements showed that the Co and $Co_{75}Pt_{25}$ exhibited almost the same absolute demagnetization values [**Figure 3(a)**]. Considering that only the fraction of g-PtCo with Pt content above ~75% lost its ferromagnetic ordering at room temperature [49], and the estimates of the magnetic dead layer thickness d_0 in the Pt/Co and Pt/g-PtCo/Co (**Table 1**), we concluded that the thickness of the layer serving as a source of spin current owing to demagnetization increased by ≈ 0.3 nm in the Pt/g-PtCo/Co compared to the Pt/Co. The above could lead to an increase in the THz emission as the effective thickness of the FM layer was closer to the optimal one reported to be ≈2 nm [15]. However, as shown in **Figure 2(b)**, the absolute demagnetization value was slightly lower for the Pt/g-PtCo/Co than for Pt/Co, signifying a lower generated spin current, which partly compensated for the effect of increasing the FM layer thickness.

The role of the gradient layer at the interface as an additional spin-to-charge converter was examined by comparing the THz waveforms of the $Co_{50}Pt_{50}$/Co and $Co_{75}Pt_{25}$/Co, where the signals had comparable magnitudes and opposite polarities [**Figure 1(d)**]. The presence of magnetic ordering at room temperature in the PtCo alloys with Pt content below ≈75% [49] allowed them to emit THz pulses owing to the ultrafast demagnetization, which competed with the contribution of the ISHE owing to the spin current injected from the Co.

The balance between these two effects depends on the composition and leads to a dominant contribution to THz emission from the ISHE in the $Co_{50}Pt_{50}$/Co and from ultrafast demagnetization in the $Co_{75}Pt_{25}$/Co. Consequently, the presence of the interfacial g-PtCo effectively increased the thickness of the layer with the ISHE, which, however, was not expected to produce enhancement of THz emission because the Pt thickness of 3 nm was close to the optimal one [15,37,50,51]. A major contribution from skew scattering within g-PtCo [25] was not expected as this layer was crystalline [36].

Therefore, we could conclude that the gradient interface between the Co and Pt layers mediated the delivery of more spin current to the Pt layer. To quantify the corresponding enhancement of the transmittance T of the interface in the Pt/g-PtCo/Co as compared to Pt/Co, a ratio between spin currents $J_s \propto T\Delta M$ [26,45] in the Pt in the two samples was evaluated. Based on the formalism in Ref. [37], J_s can be related to $E_{\mathrm{THz}}^{\mathrm{peak}}$ as follows:

$$E_{\mathrm{THz}}^{\mathrm{peak}} \propto T\Delta M \tanh\left(\frac{d_{\mathrm{FM}}-d_0}{2\lambda_{\mathrm{pol}}}\right)\tanh\left(\frac{d_{\mathrm{NM}}}{2\lambda_{\mathrm{NM}}}\right) \times Z \exp\left(-\frac{d_{\mathrm{FM}}+d_{\mathrm{NM}}}{S_{\mathrm{THz}}}\right), \quad (1)$$

where

$$Z = \frac{Z_0}{n_{\mathrm{air}} + n_{\mathrm{Si}} + Z_0(\sigma_{\mathrm{FM}}d_{\mathrm{FM}} + \sigma_{\mathrm{NM}}d_{\mathrm{NM}} + \sigma_{\mathrm{Ta}}d_{\mathrm{Ta}})}.$$

Here, λ_{pol} denotes the critical thickness of the FM layer above which the generated spin polarization saturates [37], λ_{NM} is the spin diffusion length in the NM layer, Z_0 stands for the free space impedance, n_{Si} is the optical index of the substrate, σ_m (m = FM, NM, Ta) denotes the conductivity of the layer, and d_m is its thickness.

In Pt/g-PtCo/Co, d_{FM} stands for the total thickness of Co and the gradient interface. A typical value of the effective inverse absorption constant, S_{THz} coming from multiple reflections in metal structures was used. All the parameters used in the calculations are listed in **Table 2**.

The dependences $E_{\mathrm{THz}}^{\mathrm{peak}}$ (ΔM) for the Pt/g-PtCo/Co and Pt/Co samples are shown in **Figure 3(b)**, as obtained from the fluence dependences of these values interpolated by the exponential functions $1 - A\exp(-F)$ [**Figures 3(a), 3(c)**]. Using these data, **Equation (1)**, and assuming that the spin Hall angle in the Pt layer was the same in the two samples, we could obtain a ratio T_G/T_S between the spin transmittance of the gradient interface T_G in the Pt/g-PtCo/Co and of the abrupt interface T_S in the Pt/Co at different degrees of demagnetization ΔM [as shown by the purple line in **Figure 3(b)**]. Moreover, $T_G/T_S \approx 3$ at low demagnetization, with the gradient interface allowing a pronounced increase of the injected spin current into the Pt layer. However, as the degree of demagnetization increased, T_G/T_S steadily decreased.

The latter could be ascribed to spin accumulation in the NM layer, which limited the growth of the spin current in this layer [28]. Indeed, in heavy-metal layers, the injection of spin-polarized electrons results in spin accumulation because of relatively low electron mobility. In the limiting case of a strong spin current, spin accumulation prevents a further increase in the injected spin current. Thus, the transmittance which connects J_s and ΔM is effectively reduced with increased spin accumulation. The decrease in T_G/T_S indicates that

spin accumulation was more pronounced in Pt/g-PtCo/Co, which resulted from the higher initial transmittance T_G of the interface in this structure.

A characteristic signature of the spin accumulation affecting the spin current injected into the Pt layer is the saturation behavior of the optical fluence dependence of $E_{\mathrm{THz}}^{\mathrm{peak}}$ and THz fluence [28]. Indeed, $E_{\mathrm{THz}}^{\mathrm{peak}}(F)$ in the Pt/g-PtCo/Co and Pt/Co exhibited a tendency toward saturation, which was distinct from the dependence of the THz field generated by ultrafast demagnetization in the Co and $Co_{75}Pt_{25}$ samples [**Figure 3(c)**]. Moreover, there was a decreasing trend in the optical-to-THz fluence conversion coefficient $C(F)$, as shown in **Figure 3(d)**. The THz fluence was calculated by integrating E_{THz}^2 over the THz pulse duration divided by the irradiated area of the electro-optical crystal [47]. In both samples, the conversion decreased with optical fluence, similar to the results reported in Ref. [56]. Fitting this dependence using a reciprocal function $(c_0+d\ F)^{-1}$, we determined that the maximum conversion achievable at low fluences amounted to $2\cdot10^{-6}$ in Pt/g-PtCo/Co and $1\cdot10^{-6}$ in Pt/Co. The optics-to-THz conversion efficiency ratio C_G/C_S between the Pt/g-PtCo/Co and Pt/Co was ≈ 2 and was constant in the studied optical fluence range [as shown by the linearly fitted purple symbols in **Figure 3(d)**].

These observations can be explained as follows. On one hand, the rate of increase of the demagnetization value ΔM grows slower with optical вяfluence in the Pt/g-PtCo/Co than in Pt/Co. As a result, the increase in demagnetization became sublinear in Pt/Co at lower fluences than in Pt/g-PtCo/Co, as shown in **Figure 3(a)**. This affected the generation of spin current. However, the higher transmittance of the gradient interface in the Pt/g-PtCo/Co resulted in an overall larger spin current injected into the Pt layer and a larger spin accumulation effect. The interplay of these two effects resulted in a nearly constant ratio of optical-to-THz fluence conversion of $C_G/C_S \approx 2$. Notably, increased optical fluence led to more extensive heating of the Pt layer, which in turn affected the spin Hall angle in the Pt owing to the higher spin-dependent scattering at elevated temperatures [57]. However, this effect was expected to be similar in both samples studied, thus it did not influence the C_G/C_S and T_G/T_S ratios.

Finally, we addressed the possible connection between the increased transmittance of the gradient interface for the spin-polarized current revealed in the experiments and the recently reported increase in the interfacial DMI [36]. The transmittance is related to the average spin conductance $(g^{\uparrow} + g^{\downarrow})/2$. Ref. [26] suggested a direct correlation between the average spin conductance in an NM/FM structure and the spin-mixing conductance $g^{\uparrow\downarrow}$ of the NM/FM interface. Further, interfacial DMI and spin-mixing conductance are correlated in NM/FM structures [29]. Thus, the results reported here and those in Ref. [36] demonstrated that the gradient interface in the Pt/Co structure led to an increase in the THz emission and DMI, supporting the conclusions of these studies.

Conclusions

This study highlighted the crucial role of interface design in spintronic emitters, which dramatically affects their spin current transmittance. Using a crystalline composition-gradient interface between the ferromagnetic and heavy-metal layers led to a two-fold increase in the efficiency of the Pt/Co spintronic emitter compared with conventional heterostructures. These findings paved the way for further optimization of NM/FM emitters

by exploring the effect of the gradient steepness and thickness of the interfacial layer on the THz emission. The enhancement of the interface spin transmittance was observed alongside the increase in interfacial DMI, suggesting an intrinsic link between the spin and spin-mixing conductance values and the DMI in Pt/Co structures. The Pt/Co structure with a gradient interface supported the in-plane magnetic anisotropy required for THz emitters in combination with a small Co layer thickness, which was optimal for efficient spin current generation. This contrasts with Pt/Co structures, which were typically characterized by out-of-plane anisotropy.

Acknowledgments
The authors thank R. M. Dubrovin and E. A. Mashkovich for their helpful tips regarding the THz experiments.

Disclosure statement
The authors declare no conflict of interest.

Funding
An experimental study of THz emissions by A.V.K., L.A.Sh. and A.M.K. was supported by RScF Grant No. 23-12-00251 (https://rscf.ru/en/project/23-12-00251/). The structural characterization of the samples by A.V.T. was supported by RScF Grant No. 21-72-20160 (https://rscf.ru/en/project/21-72-20160). Magnetic characterization of the samples by A.S.S. was supported by RScF Grant No. 23-42-00076 (https://rscf.ru/en/project/23-42-00076/). A.V.O. acknowledges support from the Russian Ministry of Science and Higher Education (State Assignment No. FZNS2023–0012) as part of the magnetic domain structure investigation. Y.K.K. acknowledges the support of the National Research Foundation of Korea funded by the Ministry of Science and ICT (RS-2023-00258680).

ORCID

L. A. Shelukhin	0000-0001-8538-3773
A. V. Kuzikova	0000-0002-6648-8817
A. V. Telegin	0000-0001-7209-4307
V. D. Bessonov	0000-0002-7837-4366
A. V. Ognev	0000-0002-1619-3666
A. S. Samardak	0000-0001-5917-4361
Junho Park	0000-0003-0294-1288
Young Keun Kim	0000-0002-0868-4625
A. M. Kalashnikova	0000-0001-5635-6186

References

[1] Park GS, Tani M, Rieh JS, et al. Advances in terahertz source technologies. Jenny Stanford Publishing; 2024.
[2] Papaioannou ET, Beigang R. THz spintronic emitters: a review on achievements and future challenges. Nanophotonics. 2020;10(4):1243–1257.
[3] Lewis RA. A review of terahertz sources. Journal of Physics D: Applied Physics. 2014;47(37):374001.

[4] Pettine J, Padmanabhan P, Sirica N, et al. Ultrafast terahertz emission from emerging symmetry-broken materials. Light: Science & Applications. 2023;12(1):133.
[5] Seifert T, Jaiswal S, Martens U, et al. Efficient metallic spintronic emitters of ultrabroadband terahertz radiation. Nature Photon. 2016;10(7):483–488.
[6] Fülöp JA, Tzortzakis S, Kampfrath T. Laser-driven strong-field terahertz sources. Advanced Optical Materials. 2020;8(3):1900681.
[7] Zhu X, Bacon DR, Madéo J, et al. High field single-to few-cycle THz generation with lithium niobate. In: Photonics; Vol. 8; MDPI; 2021. p. 183.
[8] Herink G, Wimmer L, Ropers C. Field emission at terahertz frequencies: AC-tunneling and ultrafast carrier dynamics. New Journal of Physics. 2014;16(12):123005.
[9] Wang P, Feng Z, Yang Y, et al. Inverse orbital Hall effect and orbitronic terahertz emission observed in the materials with weak spin-orbit coupling. npj Quantum Materials. 2023;8(1):28.
[10] Liu Y, Xu Y, Fert A, et al. Efficient orbitronic terahertz emission based on CoPt alloy. Advanced Materials. 2024;36(36):2404174.
[11] Agarwal P, Mishra SS, Medwal R, et al. Reconfigurable chiral spintronic THz emitters. Advanced Optical Materials. 2024;12(20):2303128.
[12] Cheng L, Li Z, Zhao D, et al. Studying spin–charge conversion using terahertz pulses. APL Materials. 2021;9(7):070902.
[13] Liu Y, Cheng H, Xu Y, et al. Separation of emission mechanisms in spintronic terahertz emitters. Phys Rev B. 2021;104:064419.
[14] Wu W, Yaw Ameyaw C, Doty MF, et al. Principles of spintronic THz emitters. J Appl Phys. 2021;130(9):091101.
[15] Seifert TS, Cheng L, Wei Z, et al. Spintronic sources of ultrashort terahertz electromagnetic pulses. Applied Physics Letters. 2022;120(18):180401.
[16] Rouzegar R, Chekhov A, Behovits Y, et al. Broadband spintronic terahertz source with peak electric fields exceeding 1.5 MV/cm. Phys Rev Appl. 2023;19:034018.
[17] Yang D, Liang J, Zhou C, et al. Powerful and tunable THz emitters based on the Fe/Pt magnetic heterostructure. Advanced Optical Materials. 2016;4(12):1944–1949.
[18] Wu Y, Elyasi M, Qiu X, et al. High-performance THz emitters based on ferromagnetic/nonmagnetic heterostructures. Advanced Materials. 2016;29(4):1603031.
[19] Agarwal P, Huang L, Ter Lim S, et al. Electric-field control of nonlinear THz spintronic emitters. Nature Communications. 2022;13(1):4072.
[20] Saitoh E, Ueda M, Miyajima H, et al. Conversion of spin current into charge current at room temperature: Inverse spin-Hall effect. Applied Physics Letters. 2006;88(18):182509.
[21] Wang L, Wesselink RJH, Liu Y, et al. Giant room temperature interface spin Hall and inverse spin Hall effects. Phys Rev Lett. 2016;116:196602.
[22] Hellman F, Hoffmann A, Tserkovnyak Y, et al. Interface-induced phenomena in magnetism. Rev Mod Phys. 2017;89:025006.
[23] Agarwal P, Medwal R, Dongol K, et al. Interfacial spintronic Thz emission. Advanced Optical Materials. 2024;12(22):2400077.
[24] Jungfleisch MB, Zhang Q, Zhang W, et al. Control of terahertz emission by ultrafast spin-charge current conversion at Rashba interfaces. Phys Rev Lett. 2018;120:207207.
[25] Gueckstock O, Nádvorník L, Gradhand M, et al. Terahertz spin-to-charge conversion by interfacial skew scattering in metallic bilayers. Advanced Materials. 2021;33(9):2006281.
[26] Hawecker J, Dang TH, Rongione E, et al. Spin injection efficiency at metallic interfaces probed by THz emission spectroscopy. Advanced Optical Materials. 2021;9(17):2100412.

[27] Zhang Q, Hikino Si, Yunoki S. First-principles study of the spin-mixing conductance in $Pt/Ni_{81}Fe_{19}$ junctions. Applied Physics Letters. 2011;99(17):172105.
[28] Kampfrath T, Battiato M, Maldonado P, et al. Terahertz spin current pulses controlled by magnetic heterostructures. Nature nanotechnology. 2013;8(4):256–260.
[29] Ma X, Yu G, Tang C, et al. Interfacial Dzyaloshinskii-Moriya interaction: Effect of 5*d* band filling and correlation with spin mixing conductance. Phys Rev Lett. 2018;120:157204.
[30] Tao X, Liu Q, Miao B, et al. Self-consistent determination of spin Hall angle and spin diffusion length in Pt and Pd: The role of the interface spin loss. Science Advances. 2018; 4(6):eaat1670.
[31] Nguyen H, Pratt W, Bass J. Spin-flipping in Pt and at Co/Pt interfaces. Journal of Magnetism and Magnetic Materials. 2014;361:30–33.
[32] Rojas-Sánchez JC, Reyren N, Laczkowski P, et al. Spin pumping and inverse spin Hall effect in platinum: The essential role of spin-memory loss at metallic interfaces. Phys Rev Lett. 2014;112:106602.
[33] Gupta K, Wesselink RJH, Liu R, et al. Disorder dependence of interface spin memory loss. Phys Rev Lett. 2020;124:087702.
[34] Li G, Medapalli R, Mikhaylovskiy RV, et al. THz emission from Co/Pt bilayers with varied roughness, crystal structure, and interface intermixing. Phys Rev Mater. 2019; 3:084415.
[35] Scheuer L, Ruhwedel M, Karfaridis D, et al. THz emission from Fe/Pt spintronic emitters with L10-FePt alloyed interface. Iscience. 2022;25(5):104319.
[36] Park J, Kim T, Kim GW, et al. Compositional gradient induced enhancement of Dzyaloshinskii–Moriya interaction in Pt/Co/Ta heterostructures modulated by Pt–Co alloy intralayers. Acta Materialia. 2022;241:118383.
[37] Torosyan G, Keller S, Scheuer L, et al. Optimized spintronic terahertz emitters based on epitaxial grown Fe/Pt layer structures. Scientific Reports. 2018;8(1):1311.
[38] Maret M, Cadeville M, Staiger W, et al. Perpendicular magnetic anisotropy in Co_xPt_{1-x} alloy films. Thin Solid Films. 1996;275(1–2):224–227.
[39] Hashimoto S, Ochiai Y, Aso K. Perpendicular magnetic anisotropy and magnetostriction of sputtered Co/Pd and Co/Pt multilayered films. Journal of Applied Physics. 1989; 66(10):4909–4916.
[40] Kampfrath T, Nötzold J, Wolf M. Sampling of broadband terahertz pulses with thick electro-optic crystals. Appl Phys Lett. 2007;90(23):231113.
[41] Gerevenkov PI, Kuntu DV, Filatov IA, et al. Effect of magnetic anisotropy relaxation on laser-induced magnetization precession in thin galfenol films. Phys Rev Mater. 2021; 5:094407.
[42] Casalbuoni S, Schlarb H, Schmidt B, et al. Numerical studies on the electro-optic detection of femtosecond electron bunches. Phys Rev ST Accel Beams. 2008;11:072802.
[43] Huisman TJ, Mikhaylovskiy RV, Tsukamoto A, et al. Simultaneous measurements of terahertz emission and magneto-optical Kerr effect for resolving ultrafast laser-induced demagnetization dynamics. Phys Rev B. 2015;92:104419.
[44] Huisman TJ, Rasing T. Thz emission spectroscopy for THz spintronics. Journal of the Physical Society of Japan. 2017;86(1):011009.
[45] Rouzegar R, Brandt L, Nádvorník L, et al. Laser-induced terahertz spin transport in magnetic nanostructures arises from the same force as ultrafast demagnetization. Phys Rev B. 2022;106:144427.
[46] Beaurepaire E, Turner GM, Harrel SM, et al. Coherent terahertz emission from ferromagnetic films excited by femtosecond laser pulses. Applied Physics Letters. 2004;84(18):3465– 3467.

[47] Jefimenko OD. Electricity and magnetism: An introduction to the theory of electric and magnetic fields. Appleton-Century-Crofts; 1966.
[48] Kefayati A, Nikolíc BK. Origins of electromagnetic radiation from spintronic terahertz emitters: A time-dependent density functional theory plus Jefimenko equations approach. Phys Rev Lett. 2024 Sep;133:136704.
[49] Polesya S, Mankovsky S, Sipr O, et al. Finite-temperature magnetism of Fe_xPd_{1-x} and Co_xPt_{1-x} alloys. Phys Rev B. 2010;82:214409.
[50] Yang D, Liang J, Zhou C, et al. Powerful and tunable THz emitters based on the Fe/Pt magnetic heterostructure. Advanced Optical Materials. 2016;4(12):1944–1949.
[51] Yang Y, Dal Forno S, Battiato M. Modeling spintronic terahertz emitters as a function of spin generation and diffusion geometry. Phys Rev B. 2023;107:144407.
[52] Yasuda H, Hosako I. Measurement of terahertz refractive index of metal with terahertz time-domain spectroscopy. Japanese Journal of Applied Physics. 2008;47(3R):1632.
[53] Zhou C, Liu Y, Wang Z, et al. Broadband terahertz generation via the interface inverse Rashba-Edelstein effect. Physical Review Letters. 2018;121(8):086801.
[54] Li HH. Refractive index of silicon and germanium and its wavelength and temperature derivatives. Journal of Physical and Chemical Reference Data. 1980;9(3):561–658.
[55] Kumar S, Nivedan A, Singh A, et al. THz pulses from optically excited Fe-, Pt- and Ta-based spintronic heterostructures. Pramana. 2021;95(2).
[56] Buryakov AM, Gorbatova AV, Avdeev PY, et al. Efficient Co/Pt THz spintronic emitter with tunable polarization. Applied Physics Letters. 2023;123(8):082404.
[57] Matthiesen M, Afanasiev D, Hortensius J, et al. Temperature dependent inverse spin Hall effect in Co/Pt spintronic emitters. Appl Phys Lett. 2020;116(21):212405.

Tables

Table 1. Main sample composition, magnetization M_s, effective uniaxial anisotropy constant K_{eff}, magnetic dead layer d_0, and DMI parameter [36]. The numbers in brackets are the layer thicknesses in nm. Negative K_{eff} corresponds to perpendicular magnetic anisotropy.

Sample	M_S	K_{eff}	d_0	DMI
	10^5 A m^{-1}	10^4 J m^{-3}	nm	mJ m^{-2}
Pt(3)/g-PtCo[a](1.2)/Co(1.2)	10.6	10.6	0.9	-0.82
Pt(3)/Co(1.2)	10.5	-31.5	0.04	-0.44
Co(4.6)	13.6	102	-	-
$Co_{75}Pt_{25}$(4.6)	9.8	-14.7	-	0.4
[a] $Co_{25}Pt_{75}$(0.4)/$Co_{50}Pt_{50}$(0.4)/$Co_{75}Pt_{25}$(0.4)				

Table 2. Material parameters used in the calculations of E_{THz}^{peak}.

λ_{Pt}	3.4 nm	[32]	S_{THz}	150 nm	[52]
λ_{Co}	0.7 nm	[53]	n_{Si}	3.42	[54]
σ_{Co}	$3\cdot10^{-3}$ (Ω nm)$^{-1}$	[26]	Z_0	377 Ω	[37]
σ_{Pt}	$4\cdot10^{-3}$ (Ω nm)$^{-1}$	[26]			
σ_{Ta}	$2.4\cdot10^{-3}$ (Ω nm)$^{-1}$	[55]			

Figures

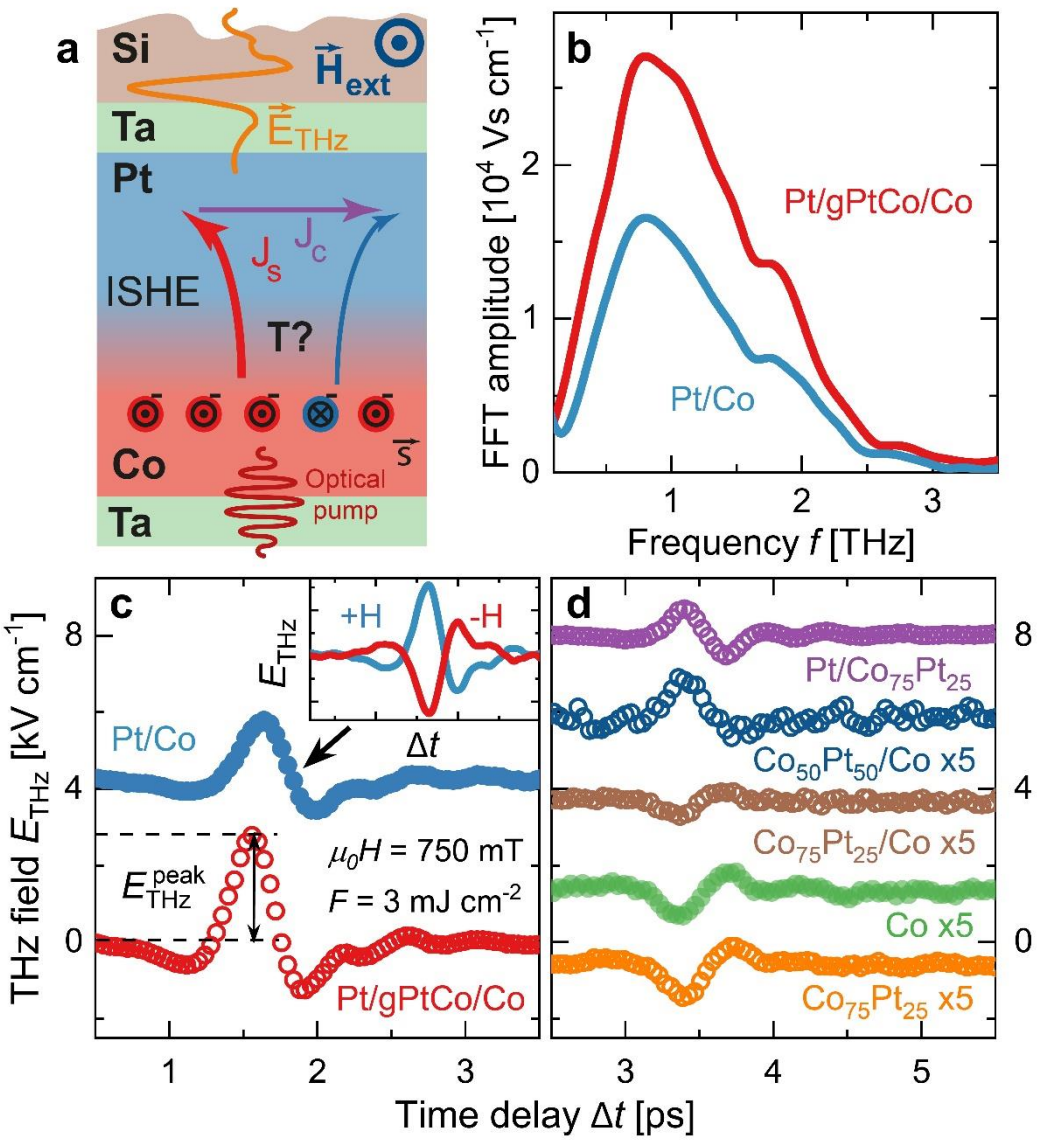

Figure 1. (a) Schematic of the generation of THz emission via the inverse Spin Hall effect in a laser-excited Pt/g-PtCo/Co structure with a composition-gradient interface. T denotes the spin transmittance of the interface between the Pt and Co layers. (b) Fourier spectra of the THz pulses generated in Pt/g-PtCo/Co (red line) and Pt/Co (blue line). Electric field temporal profile of the emitted THz pulse (c) for Pt/Co and Pt/g-PtCo/Co, and (d) Pt/$Co_{75}Pt_{25}$, $Co_{50}Pt_{50}$/Co, $Co_{75}Pt_{25}$/Co, Co, and $Co_{75}Pt_{25}$. Inset in (c) shows the THz pulse polarity inversion with the change in the external magnetic field sign.

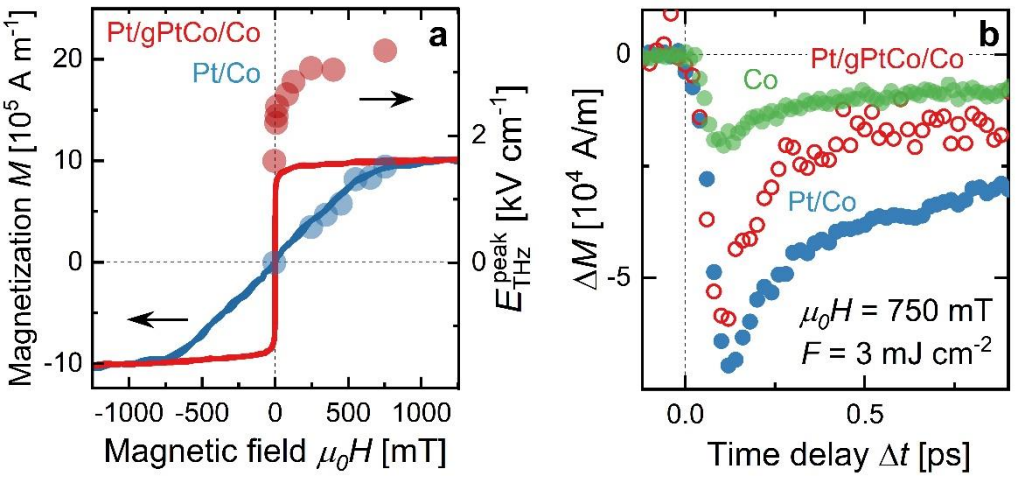

Figure 2. (a) In-plane magnetization (lines) and $E_{\mathrm{THz}}^{\mathrm{peak}}$ (symbols) obtained at F = 3 mJ · cm^{-2} as functions of the external magnetic field applied in the sample plane for Pt/g-PtCo/Co (red) and Pt/Co (blue). (b) Absolute demagnetization value as a function of the time delay (Δt) measured for the pure Co (green circles), Pt/Co (blue circles), and Pt/g-PtCo/Co (red dots) structures.

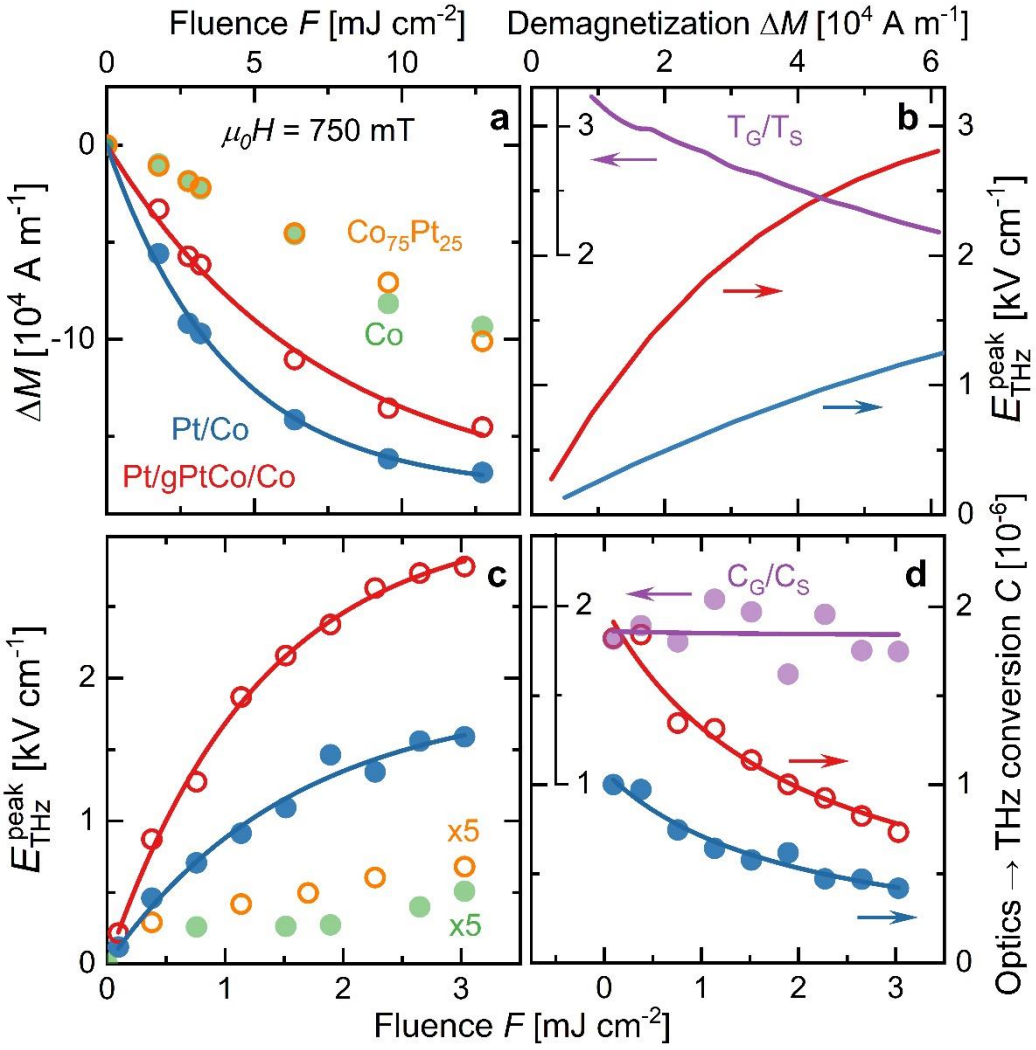

Figure 3. (a) Absolute demagnetization (ΔM) value as a function of the pump fluence. Lines are fit using an exponential function. (b) E_{THz}^{peak} as a function of the absolute demagnetization (ΔM) (right axis: red and blue lines) plotted using fit functions from panels *a*, *c*. The ratio between the interface effective transmittances of Pt/g-PtCo/Co (T_G) and Pt/Co (T_S) (additional left axis: purple line). (c) E_{THz}^{peak} as a function of the pump laser fluence measured in the external magnetic field $\mu_0 H$ = 750 mT applied in the sample plane. Lines are fit using an exponential function. (d) Conversion of the optical fluence to THz radiation of Pt/g-PtCo/Co (C_G) and Pt/Co (C_S) (right axis: red and blue symbols). Lines are fit using a reciprocal function. C_G/C_S as a function of fluence (F) using a linear fit (additional left axis: purple symbols).

Impact Statement

Pt/Co spintronic emitter with a crystalline composition gradient interface demonstrates two-fold increase of the optical-to-THz fluence conversion in comparison with a conventional Pt/Co structure with an abrupt interface. This is caused by an enhanced transmittivity of the laser-driven spin-polarized current through the gradient interface.

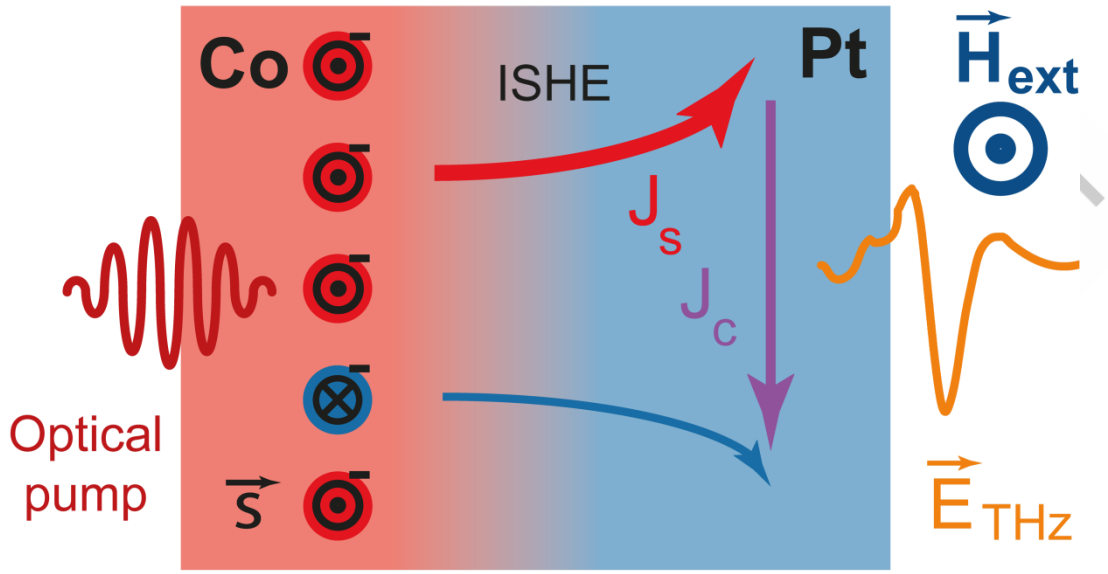

Graphical_abstract